Flat-Panel Detector–Based Volume Computed Tomography: A Novel 3D Imaging Technique to Monitor Osteolytic Bone Lesions in a Mouse Tumor Metastasis Model[1]

Jeannine Missbach-Guentner[*,†,‡], *Christian Dullin*[†], *Marta Zientkowska*[*], *Melanie Domeyer-Missbach*[*], *Sarah Kimmina*[§], *Silvia Obenauer*[†], *Fritz Kauer*[¶], *Walter Stühmer*[‡], *Eckhardt Grabbe*[†], *Wolfgang F. Vogel*[#] *and Frauke Alves*[*]

Departments of *Hematology and Oncology, and [†]Diagnostic Radiology, Georg-August-University, Göttingen 37075, Germany; [‡]Max-Planck-Institute of Experimental Medicine, Göttingen 37075, Germany; Departments of [§]Laboratory Animal Science, [¶]Traumatology, Georg-August-University, Göttingen 37075, Germany; [#]Department of Laboratory Medicine and Pathobiology, University of Toronto, Toronto, Ontario, Canada M5S 1A8

Abstract

Skeletal metastasis is an important cause of mortality in patients with breast cancer. Hence, animal models, in combination with various imaging techniques, are in high demand for preclinical assessment of novel therapies. We evaluated the applicability of flat-panel volume computed tomography (fpVCT) to noninvasive detection of osteolytic bone metastases that develop in severe immunodeficient mice after intracardial injection of MDA-MB-231 breast cancer cells. A single fpVCT scan at 200-μm isotropic resolution was employed to detect osteolysis within the entire skeleton. Osteolytic lesions identified by fpVCT correlated with Faxitron X-ray analysis and were subsequently confirmed by histopathological examination. Isotropic three-dimensional image data sets obtained by fpVCT were the basis for the precise visualization of the extent of the lesion within the cortical bone and for the measurement of bone loss. Furthermore, fpVCT imaging allows continuous monitoring of growth kinetics for each metastatic site and visualization of lesions in more complex regions of the skeleton, such as the skull. Our findings suggest that fpVCT is a powerful tool that can be used to monitor the occurrence and progression of osteolytic lesions *in vivo* and can be further developed to monitor responses to antimetastatic therapies over the course of the disease.

Neoplasia (2007) **9,** 755–765

Keywords: Flat-panel volume computed tomography, *in vivo* imaging, metastatic breast tumor model, osteolytic lesions, bone metastasis.

Introduction

The bone is the principal and frequent metastatic site in patients with breast cancer and is the most common location of the first relapse of this disease [1,2]. Many patients with bone metastases suffer from severe bone pain, and mortality is increased due to pathological fractures, nerve compression syndrome, and hypercalcemia [3]. Tumor cells invade bone cavities and secrete factors that stimulate osteoclasts to cause the resorption of cortical and trabecular bones. Multiple interactions between metastatic cancer cells and osteoclasts are slowly being uncovered, providing novel targets to design specific therapeutic interventions for bone metastases [4,5]. To understand the molecular signature of cancers that is specifically important to bone metastases and to preclinically evaluate these novel targeted therapies, the development of mouse models that mimic bone metastasis, in combination with novel imaging techniques, remains a great challenge [6].

Intracardiac inoculation of a number of different tumor types results in reproducible well-characterized bone metastases in xenograft animal models [7]. One frequently used model is based on the intracardial injection of MDA-MB-231 human breast cancer cells, consistently leading to bone but not lung metastases within a few weeks [8]. A major limitation in evaluating tumor progression in murine tumor models is the inability to detect and monitor tumor metastasis in detail over the course of the disease. The study of bone metastasis in small animal models has frequently only relied on rather cumbersome histologic analyses at the end of the study. Sacrifice of animals limits the evaluation of metastatic spread to a single time point instead of permitting individual lesions to be followed over time. *In vivo* detection of bone metastases using high-resolution radiographic analysis has been used in an attempt to provide temporal information. However, classic osteolytic lesions associated with significant bone destruction can be detected by current radiography only at

Abbreviations: SCID, severe combined immunodeficient; fpVCT, flat-panel volume computed tomography; 2D, two-dimensional; 3D, three-dimensional; H&E, hematoxylin and eosin; MRI, magnetic resonance imaging

Address all correspondence to: Jeannine Missbach-Guentner, PhD, Department of Hematology and Oncology, Georg-August-University, Robert-Koch-Str. 40, Göttingen 37075, Germany.
E-mail: j.missbach@med.uni-goettingen.de

[1]This work was supported by a grant (AL336/5-1) from the Deutsche Forschungsgemeinschaft (within SPP1190) and by a tandem grant from the Max-Planck Society.
Received 11 June 2007; Revised 20 July 2007; Accepted 21 July 2007.

DOI 10.1593/neo.07466

advanced stages, thereby leading to underestimation of the number and extent of bone metastases.

Serial micro–computed tomography (micro-CT) analysis has been used to investigate the effect of metastases on bone microarchitecture and bone strength [9–11]. Magnetic resonance imaging (MRI) has also shown potential to identify bone marrow metastases in mice before the development of cortical bone loss identifiable by X-ray [12,13]. Furthermore, nuclear medicine bone scans [14,15], skeletal scintigraphy [12], and new imaging modalities based on the optical detection of reporter genes that are bioluminescent [16] or fluorescent [17] promise to detect early events of bone metastases and to improve throughput and quantification accuracy in metastatic animal models.

In the present study, we evaluated the utility of a novel imaging technique, flat-panel volume computed tomography (fpVCT), to discover and monitor the osteolytic bone metastases of MDA-MB-231 cells in severe combined immunodeficient (SCID) mice *in vivo* over time. We demonstrate that fpVCT allows accurate localization, size determination, and assessment of the progression of lesions within the mouse skeleton, enabling rapid noninvasive detection and longitudinal monitoring of osteolytic bone lesions.

Materials and Methods

Breast Cancer Cells

The estrogen-independent human breast cancer cell line MDA-MB-231 was obtained from the American Type Culture Collection (Rockville, MD) and was cultured in Dulbecco's modified Eagle's medium supplemented with 10% fetal calf serum and 1% L-glutamine (all from PAN Systems, Aidenbach, Germany) in a humidified atmosphere of 5% CO_2 in air. Cells were regularly certified as free of *Mycoplasma* contamination. Cells were harvested to near-confluence by incubation with a 5-mM Na-EDTA solution (Gibco, Carlsbad, CA), washed several times, and placed in sterile phosphate-buffered solution shortly before implantation.

Animals

All animals were maintained under pathogen-free conditions and handled according to German regulations for animal experimentation approved by the administration of Lower Saxony, Germany. All manipulations were conducted under aseptic conditions using a laminar flow hood. For this study, SCID mice (strain C.B-17/*Ztm-scid*) were used. Immunodeficiency of SCID mice was verified by measuring serum immunoglobulin levels with enzyme-linked immunosorbent assay.

Intracardiac Experimental Metastasis Model

Six- to 10-week-old (n = 14) and 4- to 6-month-old female SCID mice (n = 7) were anesthetized with an intraperitoneal injection of 75 mg/kg ketamine hydrochloride with 15 mg/kg xylazine. Mice were injected with either 1×10^5 or 5×10^5 MDA-MB-231 cells suspended in 100 μl of sterile PBS through the intercostal space into the left ventricle of the heart using a 19-gauge needle.

Detection of Osteolytic Bone Lesions By fpVCT

Assessment of subsequent metastasis was monitored by fpVCT (GE Global Research, Niskayuna NY) either *in vitro*, by imaging isolated skeletal bones of dissected mice, or *in vivo*, by monitoring six anesthetized mice after the inoculation of 1×10^5 MDA-MB-231 cells over time on days 16, 23, 30, 37, and 43. An additional scan on day 6 and a last scan on day 42 were performed with mice after the inoculation of 5×10^5 cells.

For this purpose, mice were anesthetized with vaporized isoflurane at 1.5% to 2% concentration throughout an imaging session, centered on the fpVCT gantry axis of rotation, and placed perpendicular to the *z*-axis of the system, so that it was possible to scan the whole mouse with one rotation. fpVCT consists of a modified circular CT gantry and two amorphous silicon flat-panel X-ray detectors, each of 20.5×20.5 cm^2 with a 1024×1024 matrix of 200-μm detector elements. fpVCT works with a step-and-shoot acquisition mode. The standard *z*-coverage of one step is 4.21 cm. This system allows the acquisition of real isotropic volume data sets with a resolution of about 150 to 200 μm for high-contrast structures such as bones. All data sets were acquired with the same protocol: 1000 projection images per rotation, 8-second rotation time, 360 used detector rows, 80 kVp, and 100 mA. A modified Feldkamp algorithm implemented on an eight-node simultaneous computer was used for image reconstruction resulting in high-resolution volume data sets (512×512 matrix), which were analyzed with voxtools 3.0.64 Advantage Workstation 4.2 (GE Healthcare, Buckinghamshire, UK). To suppress digitalization artifacts, the isotropic voxel size of reconstructed volume data sets was about 100 μm less than the resolution of the system. Mice were sacrificed at the end of the 6-week observation period, and bones containing osteolytic lesions were dissected and analyzed by Faxitron analyses and histology.

Detection of Osteolytic Bone Lesions By Radiography and Histology

To confirm the presence of osteolytic lesions, radiographs of either isolated legs or dissected mice were taken using Faxitron (Faxitron model 43855; Hewlett Packard, Palo Alto, CA), with the following parameters: 36 kV, 0.3 mA of tube current, and 6 minutes of exposition. For histologic analysis, the legs of dissected mice were either embedded in methylmethacrylate as described before [18] or decalcified in Na-EDTA and processed for paraffin embedding. Five-micrometer serial sections were obtained and stained with hematoxylin and eosin (H&E).

Results

Detection of Osteolytic Lesions By Radiographic Techniques and Histology In Vitro

To detect tumor osteolysis in our initial experiments, limb bones were dissected from eight mice following the inoculation of 5×10^5 MDA-MB-231 cells in the left ventricle for 28 days. Imaging with fpVCT demonstrated the presence of distinct radiolucent osteolytic lesions in the distal femur, proximal tibia, and proximal humerus in three of eight mice

(Figure 1, *A* and *E*). The presence of these osteolytic lesions was confirmed by Faxitron X-ray analysis, which revealed tumor-induced bone lesions as radiolucent foci (Figure 1, *B* and *H*). To rule out that a process other than metastatic growth of tumor cells caused these osteolytic lesions, histologic examination was used to verify the presence of tumor cells precisely at the location of radiolucent skeletal elements (Figure 1, *C* and *D*) and to confirm the destruction of the corticalis by invading tumor cells (Figure 1, *F* and *G*).

Progressive Formation of Osteolytic Lesions within Complex Bone Structures In Vivo *over Time*

To monitor the onset and progression of bone lesions over time, six mice were inoculated intracardially with 1 ×

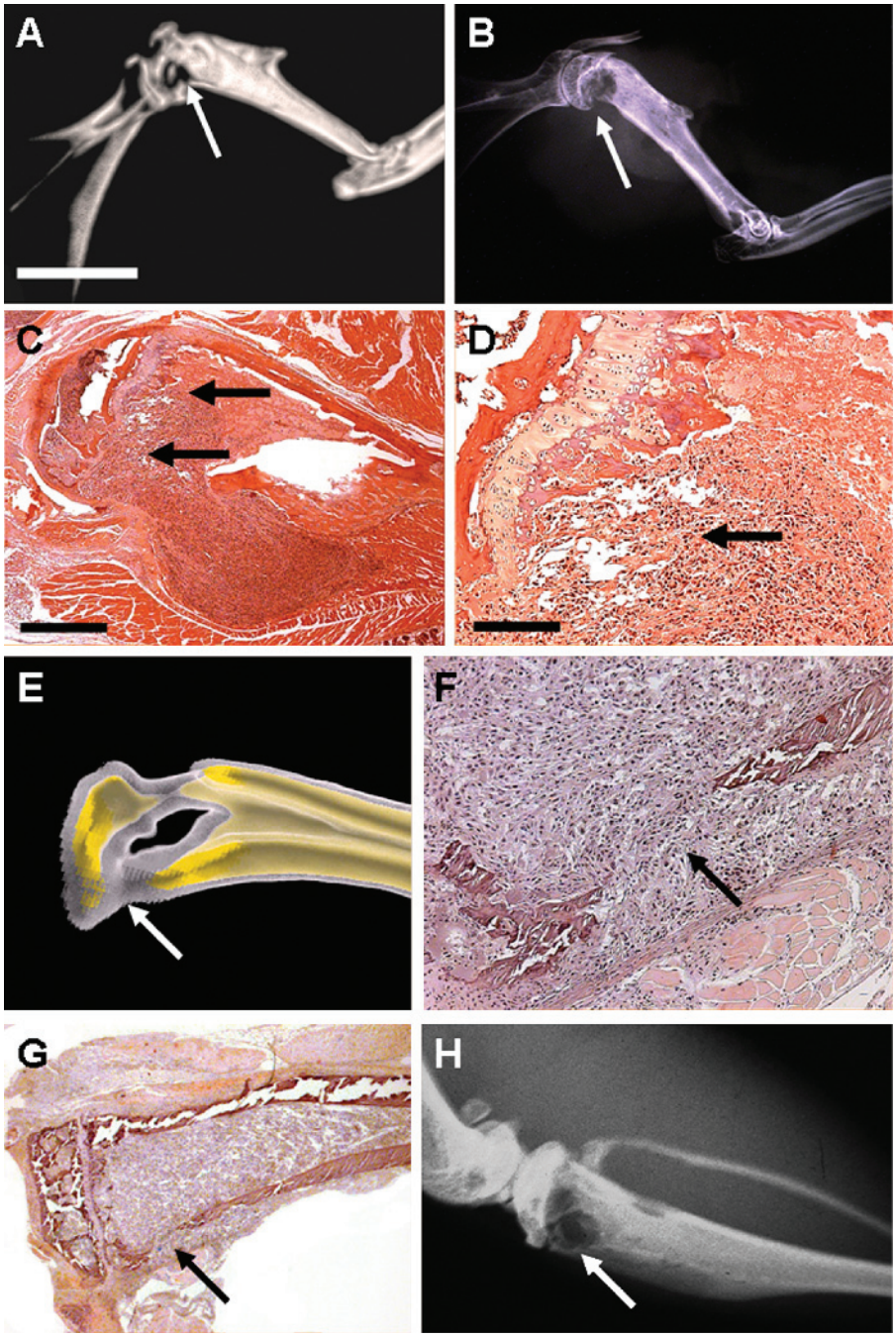

Figure 1. *Detection of an osteolytic lesion after intracardial implantation of MDA-MB-231 cells. (A) Volume rendering of a distal humerus with fpVCT 28 days after tumor cell injection demonstrates an osteolytic lesion within the cortical bone (white arrow). (B) Confirmation of the findings (white arrow) by standard radiographic examination with Faxitron X-ray. (C and D) A representative histologic section stained with H&E confirmed the presence of mammary carcinoma cells in the bone cavity with cortical destruction. Tumor cells infiltrate the bone cavity and replace hematopoiesis (black arrows). (E) Volume rendering of a 3D data set of a dissected proximal tibia embedded in methylmethacrylate with complete destruction of the corticalis (arrow). (F and G) H&E staining of the histologic section confirms the destruction of the corticalis by invading tumor cells. (H) Comparable depiction of osteolysis (arrow) with Faxitron analysis. The length of the bar in (A) represents 4 mm: 800 μm (C) and 200 μm (D).*

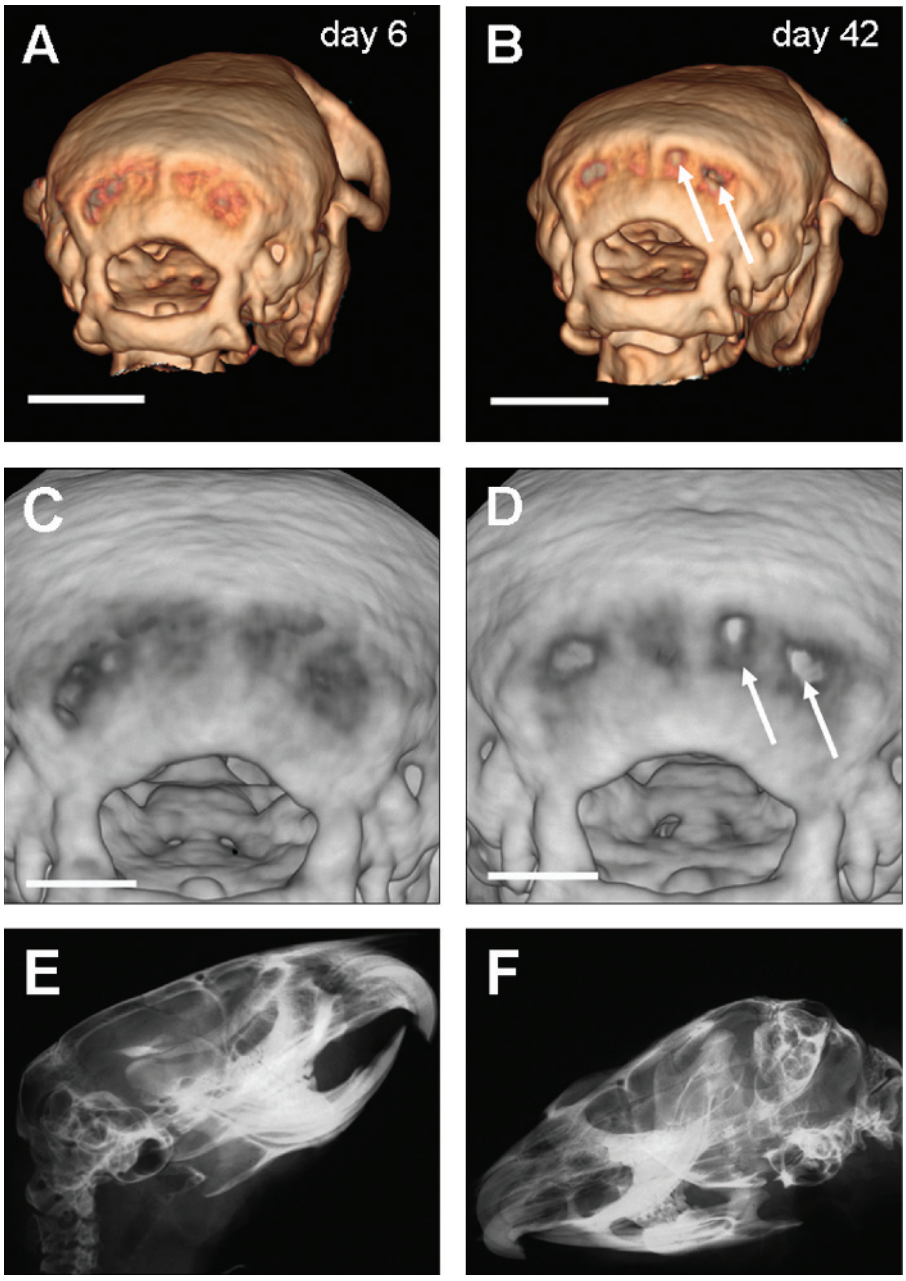

Figure 2. *Detection of osteolytic lesions within the skull* in vivo *over time. (A and B) The presence of osteolytic lesions within the skull (white arrows) is depicted by noninvasive imaging with fpVCT from the time of the intracardial inoculation of MDA-MB-231 cells. (C and D) A higher magnification of the same area of the skull clearly depicts, after 42 days (white arrows), two radiolucent areas within the occipital bone of a SCID mouse that are not visible on an fpVCT image after 6 days. The (E) lateral and (F) dorsal views of the 2D radiogram of a Faxitron analysis of the same mouse dissected after 42 days depict no bone lesion within the complex anatomic structure of the skull. The lengths of the bars in (A) and (B) represent 4 mm (C) and (D) 2 mm.*

10^5 MDA-MB-231 cells, and seven mice were inoculated with 5×10^5 MDA-MB-231 cells.

Anesthetized animals were monitored with fpVCT within 8 seconds at several time points to identify osteolytic lesions within the entire skeleton. *In vivo* analysis of the presence and progress of tumor osteolysis revealed that even in the complex anatomic structure of the skull (Figure 2, *A–D*), osteolytic lesions could be visualized by high-resolution three-dimensional (3D) fpVCT imaging demonstrating a high anatomic detail of bone structures. Because structures of low density are present even in the normal skull, only a comparison of fpVCT images with scans taken on day 6 of the study confirmed that the skeletal alterations observed in the skull have developed over time and are, therefore, most likely caused by metastases within the occipital area (Figure 2, *C* and *D*). In contrast, Faxitron analysis on the day of dissection showed projectional overlap of various bone structures and was, therefore, not able to detect osteolytic lesions within the complex skull structure (Figure 2, *E* and *F*).

Of six mice inoculated with 1×10^5 MDA-MB-231 cells, osteolytic lesions were detected either in the tibia or in the humerus of three mice. Four mice of the second group, which

were inoculated with 5×10^5 MDA-MB-231 cells, showed osteolytic lesions in the skull, in the distal humerus, or in the proximal tibia/knee.

Monitoring of the Development and Progression of Osteolytic Lesions

To noninvasively assess the progression of osteolytic lesions, fpVCT images of the whole skeleton of anesthetized mice were taken at distinct time points within 8 seconds. Axial images, as well as multiplanar reconstruction and volume-rendering images, were obtained to exhibit lesions on the bone surface, as well as the extension of osteolysis. A semitransparent volume-rendering image displayed precisely the corticalis of the tibia and, therefore, allowed the assessment of the integrity of the corticalis (Figure 3). 3D images of fpVCT data sets revealed that 23 days after intracardial inoculation of MDA-MB-231 cells, a small bone defect can be depicted in the metaphyseal region of the proximal tibia of the living mouse (Figure 3*B*), in comparison to day 16 when only a minor corticalis defect was visible at that site (Figure 3*A*). Progression of the osteolytic lesion was observed on days 30, 37, and 43, when the corticalis defect becomes more visible (Figure 3, *C*–*E*). After day 30, the osteolytic lesion had expanded and destroyed large parts of the corticalis (Figure 3*D*). Finally, the enlarged osteolytic bone metastasis is delineated within the proximal tibia (Figure 3*E*). The corresponding conventional radiograph of the tibia of the dissected mouse on day 43 confirmed the presence of the osteolytic lesion (Figure 3*F*). From fpVCT data sets, maximum intensity projection can be generated in each orientation. These images are, therefore, comparable to conventional radiography images, which are most advantageous for visualizing metastases involving surface-elongated bones (Figure 3*G*). Two-dimensional (2D) visualization of a slice through the osteolytic lesion by fpVCT confirmed massive bone lysis with corticalis destruction on day 43.

In contrast to the presentation of radiolucent foci by conventional radiographs, 3D data sets of an fpVCT image allow visualization of the bone lesion in infinitely variable angles (Figure 4, *A*–*D*). Thus, the extension of bone destruction within the cortex of the compact bone can be assessed. As shown in Figure 4*D*, the osteolytic lesion has destroyed the corticalis of the lateral and inner sites of the proximal tibia, resulting in an extensive cavity within the bone. The high-resolution volume data sets obtained by fpVCT are superior to Faxitron analysis because they can be used to generate virtual tomographic sections through the tibia with a thickness of < 200 μm in all desired orientations. Thus, the entire extension of the lesion within the bone can be assessed and revealed that only a small intact margo anterior is left (Figure 4, *E*–*H*). In contrast, standard Faxitron analysis only allows visualization of the bone in a very limited number of planes because isolated bones or mice can only

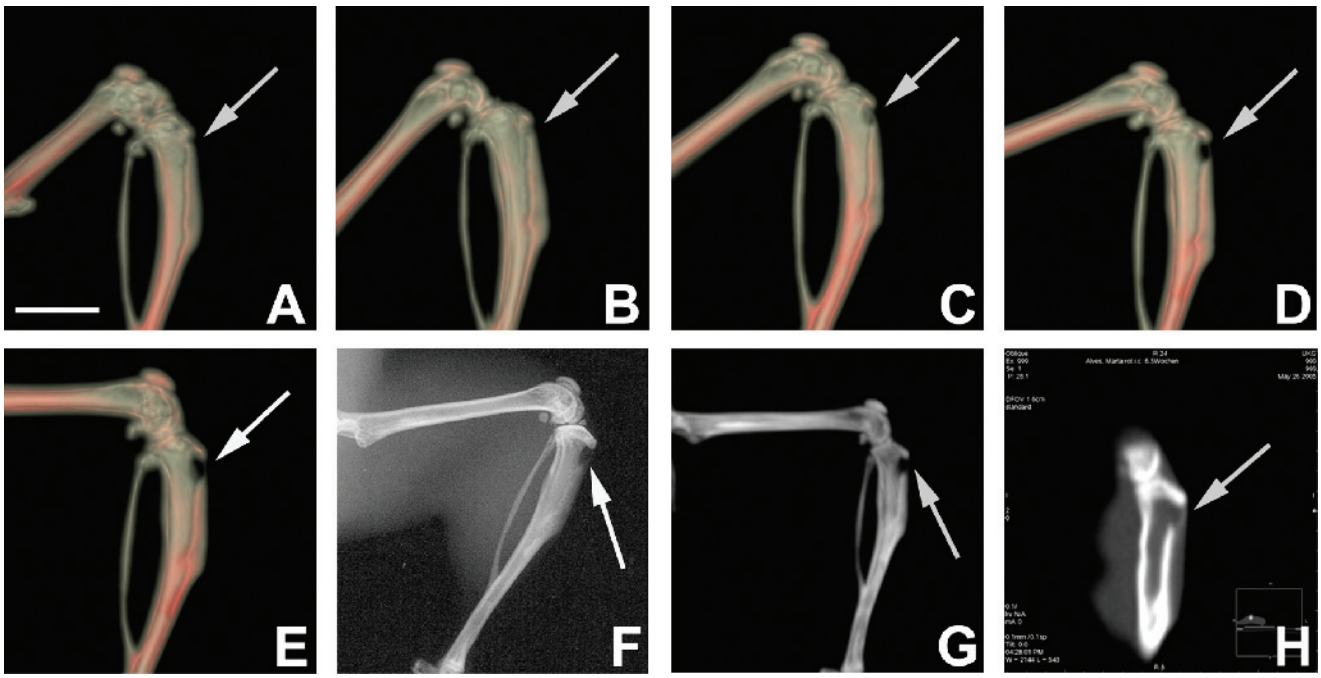

Figure 3. *Longitudinal study of the development and progression of an osteolytic lesion within the tibia of a SCID mouse. Representative fpVCT 3D images of the tibia of a SCID mouse at distinct time points from the time of the intracardial inoculation of MDA-MB-231 cells are shown (A) after 16 days, when a minor bone defect is visible; (B) after 23 days, when a small bone lesion can be depicted in the tibia (arrow); (C) after 30 days, when an osteolytic lesion with a small corticalis defect is illustrated (arrow); (D) after 37 days, when the osteolytic lesion expands and completely destroys the corticalis; and after (E) 43 days, when the enlarged osteolytic bone metastasis is delineated within the tibia. Note that the corticalis is depicted as a red shaded line. (F) A corresponding conventional radiograph of the tibia of the dissected mouse on day 43 confirmed the presence of the osteolytic lesion (arrow). (G) Maximum intensity projection of the fpVCT scan on day 43 showed similar image content such as Faxitron. (H) 2D visualization of a slice through the osteolytic lesion by fpVCT. The length of the bar in (A) represents 4 mm.*

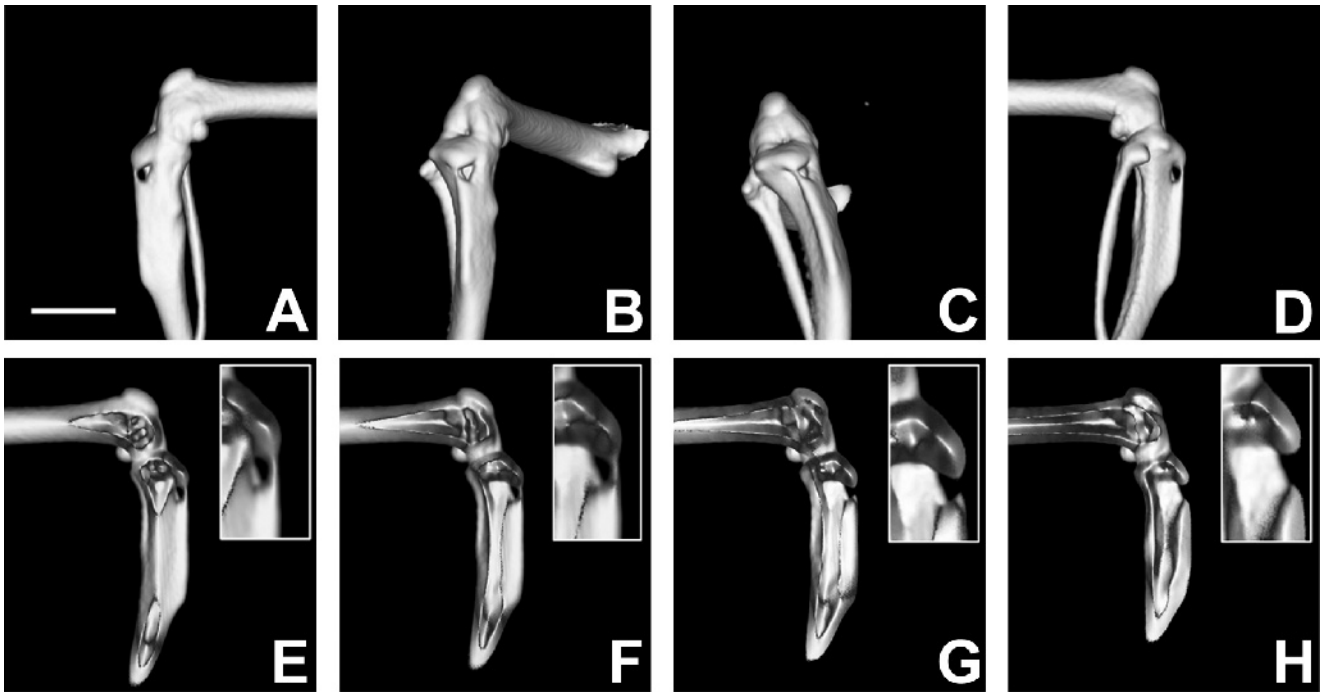

Figure 4. *Evaluation of the osteolytic lesion in arbitrary planes and virtual sections by fpVCT imaging. Representative 3D data sets of the fpVCT images of the tibia of a SCID mouse 43 days after intracardial injection of MDA-MB-231 cells allow the visualization of the osteolytic lesion within the tibia in infinitely variable angles (A–D). (E) The bone surface shows a distinct lesion with an intact margo anterior. (F–H) The entire extension of the bone lesion can be assessed by virtual slices through the destroyed corticalis toward the bone cavity. It seems that the bridge of the margo anterior prevents the bone from being fractured. The length of the bar in (A) represents 4 mm.*

be placed at limited positions, as much as possible parallel to the X-ray film to avoid a reduction in resolution.

Assessment of the Extension and Growth Rate of the Osteolytic Lesion over Time By fpVCT Imaging

High-resolution imaging by fpVCT allows measurements of distances with a precision of 200 μm in two dimensions of the osteolytic lesion within the tibia and, therefore, assessment of the growth rate and dimension of the destroyed bone area from the time of tumor implantation. Because the compact bone is completely destroyed in the third dimension, only the surface area of the bone lesion can be determined. The developing osteolytic cavity within the proximal tibia leads to two distinct apertures: one on the inner site and one on the lateral site of the tibia. As shown in Figure 5, the area of destroyed bone surface on the lateral site of the right tibia increased from 0.070 to 0.118 mm^2 on days 30 to 37 and was more than double in size 1 week later, with an area of 0.251 mm^2. The osteolytic aperture of the inner site of the tibia was visualized first on day 37 with an area of 0.079 mm^2 and increased exponentially 1 week later on day 43 to a size of 0.141 mm^2.

Furthermore, virtual tomographic sections were used to view bone defects from the inside of the bone (Figure 5, *G* and *H*), allowing 2D measurements of the area of bone destruction. By doing so, the full extension of the osteolytic lesion during tumor progression could be assessed. Both osteolytic lesions in the corticalis of the tibia that become manifest outside of the tibia extend nearly exponentially, although aperture on the left side appeared earlier.

Measurement of the diameters of the corticalis in cross sections of the fpVCT images of the affected right tibia at the same distance to the knee over time revealed not only bone and corticalis defects at the metastatic site but also reduced thickness of the corticalis (0.1 mm) at the opposite site after 43 days in comparison to day 16 (Figure 6, *A* and *B*). This demonstrates that tumor cells have already extended to within the medulla of the tibia and have affected other parts of the bone that are not as visible as osteolytic lesions. In comparison, the healthy left tibia showed no alteration in corticalis thickness at the same time points and in the same locations (Figure 6, *C* and *D*).

Changes in Bone Mass and Density Ratios of the Tibia over Time

To precisely assess the degree of damage, and hence loss of bone mass, caused by metastasis, we automatically analyzed total bone volumes at different time points by virtually isolating both tibias from fpVCT data sets. The increasing total volumes of the tibias due to the growth of mice over time were corrected under the assumption that the volume of the left tibia is constant, with a total bone volume of 36.55 mm^3. As shown in Figure 7*A*, the total bone volume of the tumor-burdened right tibia decreases progressively by about one third over 27 days (from 39.98 to 26.71 mm^3), whereas the volumes of the left tibia remained unchanged over time.

Histograms generated from fpVCT data sets of the segmented tibia with the osteolytic lesion represent the percentage of the total volumes of the tibia *versus* its measured

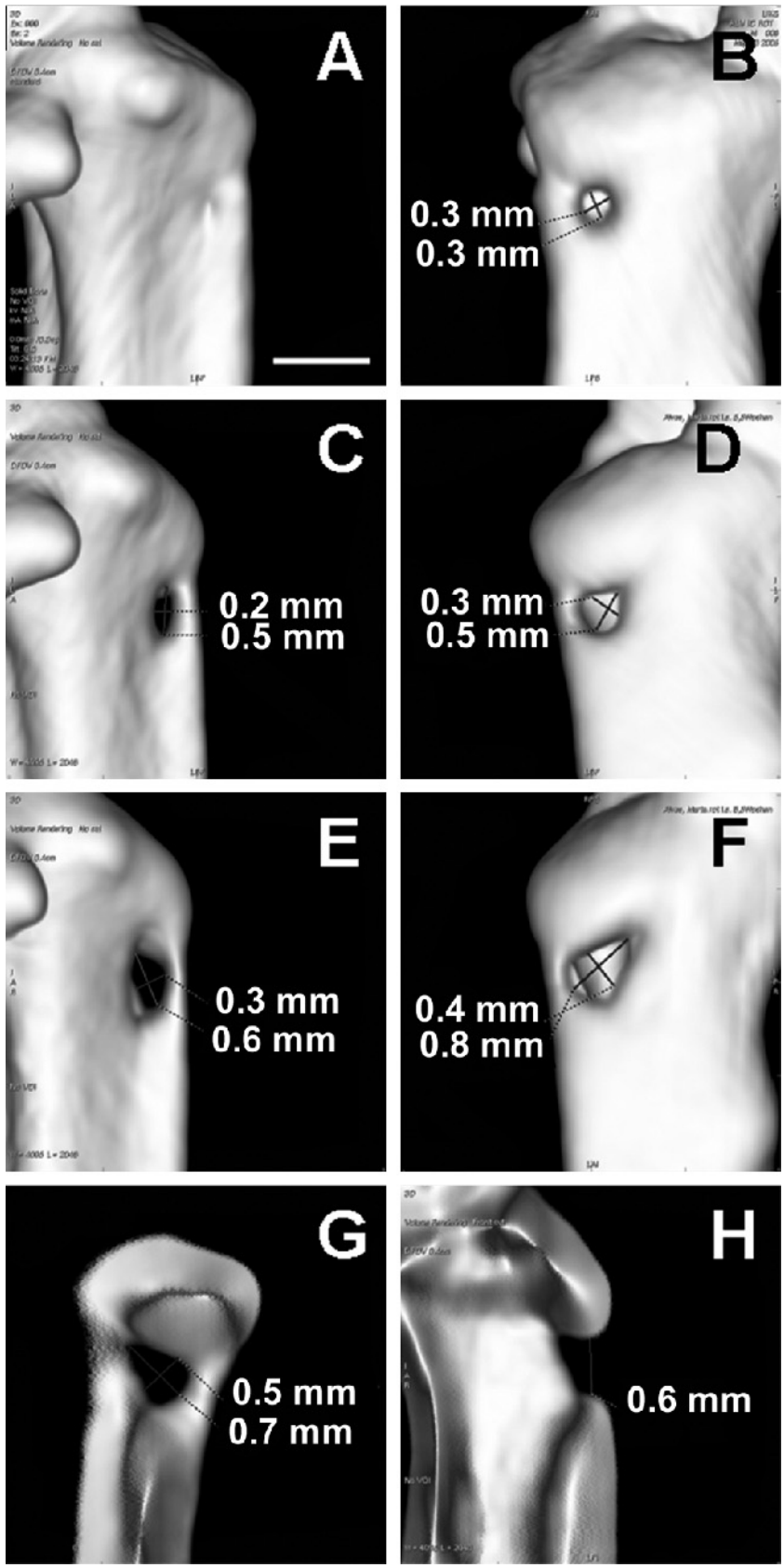

Figure 5. *Monitoring of the growth rate of the osteolytic cavity over time by fpVCT imaging. High-resolution imaging by fpVCT allows measurements of distances in two dimensions of the osteolytic lesion within the tibia from the time of tumor implantation. (A) Right lateral view of the tibia and (B) left lateral view of the tibia after 30 days; (C) right lateral view of the tibia and (D) left lateral view of the tibia after 37 days; (E) right lateral view of the tibia and (F) left lateral view of the tibia after 43 days. (G and H) Virtual sections applied to a volume-rendering fpVCT image of the tibia allow the measurement of distances in two dimensions within the bone lesion. (G) View from the bone marrow to the wall of the corticalis, and (H) frontal section through the osteolytic cavity in a left lateral view, both images after 43 days. The length of the bar in (A) represents 1 mm.*

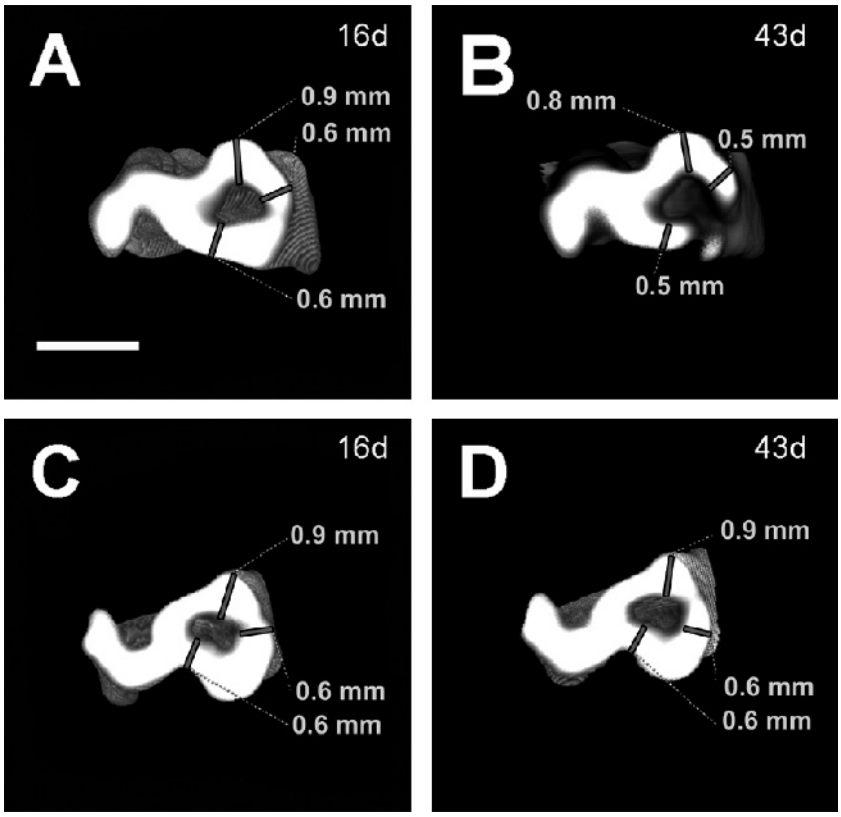

Figure 6. *Assessment of the osteolytic lesion and of the corticalis within the tibia. Representative cross sections of the fpVCT images of both tibias from the time of tumor cell injection. Measurements of the diameters of the corticalis of the (A) right tibia and the (C) left tibia on day 16, in comparison to the (B) corticalis of the right tibia with an osteolytic lesion and the (D) left tibia on day 43. Note the corticalis defect and the decreased diameters of the corticalis on day 43 in comparison to day 16. The length of the bar in (A) represents 2 mm.*

densities in Hounsfield units (HU) at two time points (Figure 7, *C* and *D*). Quantitative distribution of densities within the tibia volume can be depicted. High-density bone is represented by > 1500 HU, whereas regions of low density represent the medulla, which is composed of a network of trabecular structures.

The histogram of day 16 is composed of two underlying distributions of different density portions, which represent the corticalis region and the region of the medullary cavity composed of trabecular structures (Figure 7*C*). On day 43, the alteration of the histogram clearly depicts a loss of the high-density portions of the bone, with a simultaneous increase in bone material with density lower than that of the corticalis, suggesting partial resorption of the corticalis (Figure 7, *C* and *D*) and corresponding to our findings that wide-ranging degradation toward the inner corticalis takes place as shown in Figure 6. The loss of volume of the entire tibia bone mass corresponding to the extending osteolysis of the inner corticalis (Figure 6, *A* and *B*) is in accordance with the declining area of the histogram. This comparative analysis of histograms at two time points clearly shows that bone lesion progresses by destroying corticalis structures.

Discussion

In this study, the utility of a novel method to noninvasively analyze metastatic spread to the skeleton is shown by applying experimental volume CT with flat-panel detectors to the common bone metastasis model that requires intracardial inoculation of human MDA-MB-231 estrogen-independent breast cancer cells. Noninvasive methods are needed preclinically to understand tumor biology and to evaluate antimetastatic therapy for bone metastases that are often associated with breast cancer.

We could show that high-resolution 3D imaging allows detailed visualization of the mouse skeleton and, therefore, shows excellent sensitivity in detecting skeletal lesions at the osteolytic stage of the disease. Bones can be well depicted by fpVCT even without contrast media because of their favorable contrast properties. Therefore, fpVCT allows, in short scan times of 8 seconds, the imaging of the whole skeleton of mice and, hence, accurate anatomic localization of osteolytic lesions within the metaphyseal and diaphyseal cortical bones of the lower and upper legs, as well as in regions of the skeleton such as the skull in which lesions can hardly be visualized by standard Faxitron analysis. In the latter, isolated bones of mice can only be placed at certain positions to the X-ray film. Therefore, visualization of the bone is limited to a low number of planes, and overlap of bone structure occurs frequently.

Unlike radiography, fpVCT is a rapid and cost-effective imaging method that provides 3D representation in which bone structures are better visualized without projectional overlap. MRI has been shown to delineate the tumor itself

within the bone cavity [12,13,19]. Both fpVCT and radiography are only able to detect tumor metastases on loss of mineralized tissues in response to tumor-induced osteolysis. In contrast, MRI has been used to depict tumor progression directly within the bone marrow cavity [12,13]. Furthermore, optical imaging with fluorescently labeled antibodies has successfully been applied for the early detection of tumor cells at the site of metastasis within the bone. As an example, it was shown that fluorescence imaging of live animals allowed the detection of the intramedullary tumor growth of green fluorescent protein–labeled cells approximately 1 week before the occurrence of radiologically distinct osteolytic lesions [19]. Similarly, luciferase-transfected cells, in combination with whole-body bioluminescent imaging, were used to detect microscopic bone metastases of approximately 0.5 mm^3 [16,17,20].

In contrast, fpVCT is of great advantage in monitoring the extent of osteolytic lesions. Compared with optical imaging and MRI, fpVCT has a much better 3D resolution, especially for high-density structures, and thus provides the ability for a more accurate assessment of the extent of bone destruction.

Another method performed to evaluate bone metastases is skeletal scintigraphy using [^{99m}Tc]methylene diphosphate, which mimics calcium phosphate then becomes incorporated into regions of active bone turnover [13]. However, in small animals, this method has a relatively poor spatial resolution compared to fpVCT. Nuclear medicine bone scans are also sensitive to detecting osteoblastic bone metastases but may miss small lesions with diameters of < 1 cm^3 and may lack specificity [14,21].

The delineation of the anatomic details of bone structures in mice has been previously described for fpVCT imaging [22–25], as well as for micro-CT [26]. Micro-CT was also used to visualize experimental multiple bone metastases in the intact living mouse with serial long scanning times of about 12 minutes. Therefore, micro-CT, in comparison to fpVCT, is more invasive with respect to radiation dose and anesthesia, and is more susceptible to motion artifacts [9,10]. However, due to its high resolution of $\leq$ 50 μm, micro-CT is superior to fpVCT in the evaluation of fine trabeculae structure and microarchitecture [27]. In this study, we could demonstrate that the 200-μm resolution of fpVCT is sufficient to detect minor bone lesions in various areas of the skeleton.

It has been standard practice to monitor bone metastases using conventional radiography and bone histomorphometry performed at the end of the experiments. Histologic analysis performed to search for metastases within the whole

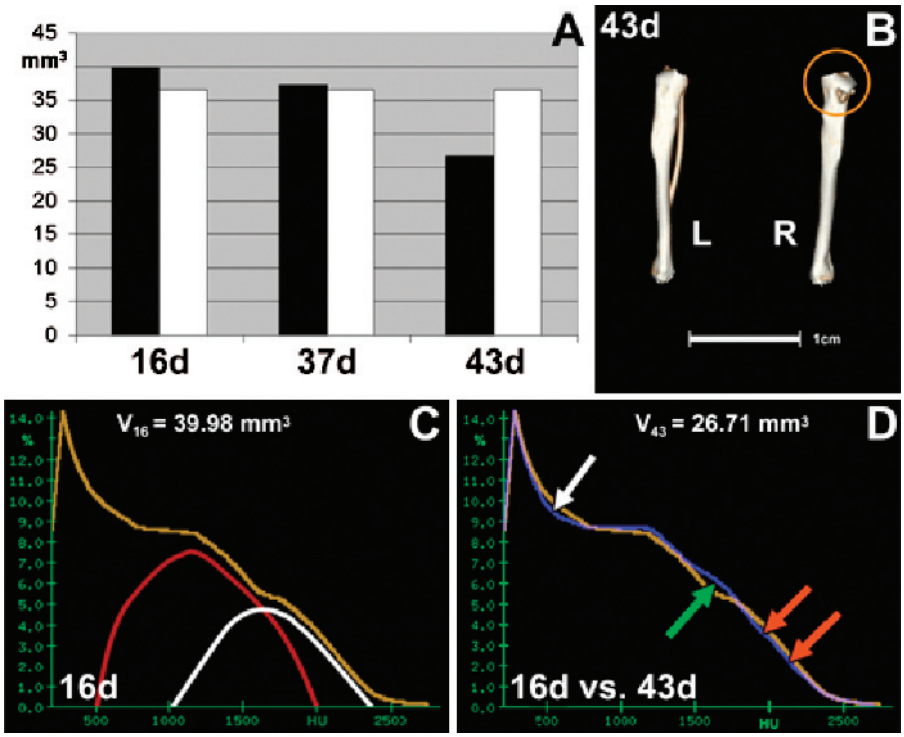

Figure 7. *Measurement of total bone volumes and the density ratios of the tibia over time. (A) The diagram shows the decrease of the total bone volume of the right tibia containing the bone lesion (black bars) in comparison to the left tibia (white) over time, 16, 37, and 43 days after the implantation of MDA-MB-231 cells. (B) Volume-rendering representation of the right and left tibiae scanned with fpVCT on day 43. A massive bone defect is depicted in the right tibia (circle). (C and D) Histograms of X-ray attenuation distributions are displayed and measured in Hounsfield units for the segmented right tibias (C) on day 16 and (D) day 43. (C) A typical graph seen in the histogram of the tibia at the early time point is the result of the summation of underlying distributions for the bone marrow with a low density (< 500 HU), with the region of the medullary cavity composed of trabecular structures (red curve), and the corticalis region (white curve) with a high density. (D) Overlay of the histogram on day 16 (yellow) and the histogram 1 day before dissection (blue). At the time when tumor osteolysis occurs, loss of bone mass, which can be determined exactly, is illustrated in a slight reduction of low-density portions (most likely representing the bone marrow) (white arrow) caused by invading tumor cells. In comparison to the early time point, the graph of the histogram on day 43 (the clear distribution of the compartments of the corticalis and the trabecular structures) becomes indistinct as result of an increase in bone with medial density (green arrow) and a decrease in bone with high density (orange arrows), suggesting that the bone lesion progresses by destroying corticalis structures.*

skeleton is typically difficult and extremely laborious. Therefore, imaging methods performed to determine osteolytic lesions are highly desirable. In comparison to standard Faxitron X-ray, fpVCT is superior because it obtains true isotropic 3D volume data sets to evaluate the skeleton in arbitrary planes and in virtual tomographic sections. Visualization of bone lesions and virtual cross sections with a thickness of 200 μm from various angles, as well as from inside the bone, permits the assessment of the complete extension of the osteolytic lesion by viewing the defect from the inner or the outer site of the bone. Furthermore, various 3D visualization techniques can be applied to fpVCT data sets, such as semitransparent volume rendering and maximum intensity projection. This allows a precise analysis of the osteolytic lesion within the corticalis or gaining of information on the exact location of the lesion within the bone.

Another advantage of fpVCT is the chance to repeat it several times *in vivo* and, therefore, to monitor tumor burden in the bone of living animals throughout the course of the experiment. When evaluating therapeutic efficacy, fpVCT might allow to identify and use only the subset of animals that had developed bone lesions, as well as to follow an individual lesion longitudinally. Due to precise measurements in two dimensions of the area of bone destruction at any time, the onset and progression of the bone destruction of individual bone lesions might be accurately assessed over the course of the disease. In clinical settings, monitoring metastatic bone lesions by fpVCT will provide a timely and precise measurement of the efficacy of antineoplastic therapy. Closely following tumor progression or tumor relapse is imperative for a tailored therapeutic strategy.

Measurements of corticalis thickness in cross sections allow the characterization of the extension of the destroyed bone mass by invading tumor cells. Our results clearly show that loss of bone mass is not only restricted to the osteolytic lesion itself but also affects the whole inner corticalis. Furthermore, with the ability to analyze the total volume of single bones automatically in fpVCT data sets, changes in bone mass, and hence the destruction of the whole bone caused by osteolysis, can be precisely and semiautomatically determined over time. Histograms of bones generated over time offer information on the distribution of bones containing dense portions and display bone volume as represented by the area below the curve at one time point. Changes in portions according to loss of specific bone structures such as the corticalis or medulla, as a consequence of the wide-ranging loss of bone mass, are exactly educible and will allow an understanding of the extent of tumor progression.

In summary, fpVCT may be a powerful and cost-effective tool for detecting osteolytic lesions within the skeleton of mice and for monitoring bone response to tumor cells *in vivo* over time. By assessing the precise localization and size of bone lesions in a longitudinal study, fpVCT might be applied to clinically evaluate response to antimetastatic therapies over the course of the disease and might help to optimize or change therapeutic strategy at an early stage.

Acknowledgements

The authors would like to acknowledge Roswitha Streich, Johanna Widera, and Sarah Greco for excellent technical assistance, as well as Kristin Hammer, Tomasz Karykowski, and Karin Stapp-Kurz for technical support in performing fpVCT.

References

[1] James JJ, Evans AJ, Pinder SE, Gutteridge E, Cheung KL, Chan S, and Robertson JF (2003). Bone metastases from breast carcinoma: histopathological–radiological correlations and prognostic features. *Br J Cancer* **289**, 660–665.

[2] Solomayer EF, Diel IJ, Meyberg GC, Gollan C, and Bastert G (2000). Metastatic breast cancer: clinical course, prognosis and therapy related to the first site of metastasis. *Breast Cancer Res Treat* **59**, 271–278.

[3] Coleman RE (1997). Skeletal complications of malignancies. *Cancer* **80**, 1588–1594.

[4] Yoneda T and Hiraga T (2005). Crosstalk between cancer cells and bone microenvironment in bone metastasis. *Biochem Biophys Res Commun* **328**, 679–687.

[5] Katanuma N, Tsuge H, Nukatsuka M, Asao T, and Fukushima M (2002). Structure-based design of specific cathepsin inhibitors and their application to protection of bone metastases of cancer cells. *Arch Biochem Biophys* **397**, 305–311.

[6] Rose AAN and Siegel PM (2006). Breast cancer–derived factors facilitate osteolytic bone metastasis. *Bull Cancer* **93**, 931–943.

[7] Rosol TJ, Tannehill-Gregg SH, LeRoy BE, Mandl S, and Contag CH (2003). Animal models of bone metastasis. *Cancer* **97** (Suppl 3), 748–757.

[8] Hiraga T, Williams PJ, Mundy GR, and Yoneda T (2001). The bisphosphonate ibandronate promotes apoptosis in MDA-MB-231 human breast cancer cells in bone metastases. *Cancer Res* **61**, 4418–4424.

[9] Arrington SA, Schoonmaker JE, Damron TA, Mann KA, and Allen MJ (2006). Temporal changes in bone mass and mechanical properties in a murine model of tumor osteolysis. *Bone* **38**, 359–367.

[10] Li X-F, Zanazonico P, Clifton C, and Donoghue J (2006). Visualization of experimental lung and bone metastases in live nude mice by X-ray micro-computed tomography. *Technol Cancer Res Treat* **5**, 147–155.

[11] Matheja P, Rickert C, Weckesser M, Palkovic S, Lottgen J, Riemann B, Kopka K, Kuwert T, Wassmann H, Paulus W, et al. (2000). Sequential scintigraphic strategy for the differentiation of brain tumours. *Eur J Nucl Med* **27**, 550–558.

[12] Gauvain KM, Garbow JR, Song SK, Hirbe AC, and Weilbaecher K (2005). MRI detection of early bone metastases in B16 mouse melanoma models. *Clin Exp Metastasis* **22**, 403–411.

[13] Kundra V, Ng CS, Ma J, Bankson JA, Price RE, Cody DD, Do K-A, Han L, and Navonne M (2007). *In vivo* imaging of prostate cancer involving bone in a mouse model. *Prostate* **67**, 50–60.

[14] Franzius C, Hotfilder M, Poremba C, Hermann S, Schafers K, Gabbert HE, Jurgens H, Schober O, Schafers M, and Vormoor J (2006). Successful high-resolution animal positron emission tomography of human Ewing tumours and their metastases in a murine xenograft model. *Eur J Nucl Med Mol Imaging* **33**, 1432–1441.

[15] Adams JY, Johnson M, Sato M, Berger F, Gambhir SS, Carey M, Iruela-Arispe ML, and Wu L (2002). Visualization of advanced human prostate cancer lesions in living mice by a targeted gene transfer vector and optical imaging. *Nat Med* **8**, 891–897.

[16] Jenkins DE, Hornig YS, Oei Y, Dusich J, and Purchio T (2005). Bioluminescent human breast cancer cell lines that permit rapid and sensitive *in vivo* detection of mammary tumors and multiple metastases in immune deficient mice. *Breast Cancer Res* **7**, R444–R454.

[17] Drake JM, Gabriel CL, and Henry MD (2005). Assessing tumor growth and distribution in a model of prostate metastasis using bioluminescence imaging. *Clin Exp Metastasis* **22**, 674–684.

[18] Erben R (1997). Embedding of bone samples in methylmethacrylate: an improved method suitable for bone histomorphometry, histochemistry, and immunohistochemistry. *J Histochem Cytochem* **45**, 307–313.

[19] Peyruchaud O, Winding B, Pecheur I, Serre CM, Delmas P, and Clezardin P (2001). Early detection of bone metastases in a murine model using fluorescent human breast cancer cells: application to the use of the bisphosphonate zoledronic acid in the treatment of osteolytic lesions. *J Bone Miner Res* **16**, 2027–2034.

[20] Wetterwald A, van der Pluijm G, Que I, Sijmons B, Buijs J, Karperien M, Lowik CW, Gautschi E, Thalmann GN, and Cecchini MG (2002). Optical

imaging of cancer metastasis to bone marrow: a mouse model of minimal residual disease. *Am J Pathol* **160**, 1143–1153.

[21] Winkelmann CT, Figueroa SD, Rold TL, Volkert WA, and Hoffman TJ (2006). Microimaging characterization of a B16-F10 melanoma metastasis mouse model. *Mol Imaging* **5**, 105–114.

[22] Kiessling F, Greschus S, Lichy MP, Bock M, Fink C, Vosseler S, Moll J, Mueller MM, Fusenig NE, Traupe H, et al. (2005). Volumetric computed tomography (VCT): a new technology for noninvasive, high-resolution monitoring of tumor angiogenesis. *Nat Med* **10**, 1133–1138.

[23] Greschus S, Kiessling F, Lichy MP, Moll J, Mueller MM, Savai R, Rose F, Ruppert C, Gunther A, Luecke M, et al. (2005). Potential applications of flat-panel volumetric CT in morphological and functional small animal imaging. *Neoplasia* **7**, 730–740.

[24] Obert M, Ahlemeyer B, Baumgart-Vogt E, and Traupe H (2005). Flat-panel volumetric computed tomography: a new method for visualizing fine bone detail in living mice. *Comput Assist Tomogr* **29**, 560–565.

[25] Obenauer S, Dullin C, Alves F, Missbach-Guentner J, Grabbe E, and Heuser M (2007). Flat-panel-detector–based volumetric CT: performance evaluation of imaging for skeletal structures of small animals in comparison to multislice CT. *Clin Imaging* **31**, 18–22.

[26] Weichert JP (2003). Micro-computed tomography of mouse cancer models. In EC Holland (Ed.). Mouse Models of Cancer. Wiley and Sons, Hoboken, NY, pp. 339–348.

[27] Borah B, Gross GJ, Dufresne TE, Smith TS, Cockman MD, Chmielewski PA, Lundy MW, Hardtke JR, and Sod EW (2001). Three-dimensional microimaging (MRmicrol and microCT), finite element modeling, and rapid prototyping provide unique insights into bone architecture in osteoporosis. *Anat Rec* **265**, 101–110.